A theoretical and numerical analysis of vibration-controlled modules for use in active segmented partitions

Timothy W. Leishman
Acoustics Research Group, Department of Physics and Astronomy, Brigham Young University, Eyring Science Center, Provo, Utah 84602

Jiri Tichy
Graduate Program in Acoustics, The Pennsylvania State University, Applied Science Building, University Park, Pennsylvania 16802

(Received 30 June 2004; revised 18 May 2005; accepted 10 June 2005)

Many applications of active sound transmission control (ASTC) require lightweight partitions, high transmission loss over a broad frequency range, simple control strategies, and consistent performance for various source and receiving space conditions. In recent years, researchers have begun to investigate active segmented partitions (ASPs) because of their potential to meet such requirements. This paper provides a theoretical and numerical analysis of four ASP module configurations that are candidates for these applications. Analogous circuit methods are used to provide normal-incidence transmission loss and reflection coefficient estimates for their passive and active states. The active control objective for each configuration is to induce global vibration control of various transmitting surfaces through direct vibration control of a *principal* transmitting surface. Two characteristic single-composite-leaf (SCL) configurations are unable to use the strategy effectively. However, design adjustments are investigated to improve their performances. Two double-composite-leaf (DCL) configurations use the strategy much more effectively to produce efficient global control of transmitting surface vibrations and achieve high transmission loss over a broad frequency range. This is achieved through a minimum volume velocity condition on the *source* side of each module. One DCL configuration enhances module isolation in full ASP arrays while satisfying other design and performance criteria.
[DOI: 10.1121/1.1992767]

PACS number(s): 43.40.Vn, 43.50.Ki, 43.55.Rg [KAC] Pages: 1424–1438

LIST OF SYMBOLS

B = Magnetic flux density in magnet air gap of moving-coil actuator
c = Speed of sound in fluid medium
C_{Mn} = Effective mechanical compliance of nth module element
C_{Mmn} = Effective mechanical compliance coupling mth and nth module elements ($m \neq n$)
$\hat{e}_g$ = Complex open-circuit voltage amplitude of electrical control source (signal generator)
f = Frequency
G_A = Acoustic ground (ambient reference pressure)
G_M = Mechanical ground (zero reference velocity)
I = Roman numeral representing source side of module
II = Roman numeral representing transmitting side of module
j = $\sqrt{-1}$
k = Acoustic wave number, = ω/c
$\tilde{k}$ = Complex acoustic wave number accounting for propagation losses, = $k-j\alpha$
L = Effective cavity length in double-composite-leaf modules
l = Effective length of voice coil conductor in magnet air gap of moving-coil actuator
L_E = Electrical inductance of voice coil in moving-coil actuator
m = Integer index representing given module element, = 1, 2, 3, or 4
M_{Mn} = Effective mechanical mass of nth module element
n = Integer index representing given module element, = 1, 2, 3, or 4
$\hat{p}_i$ = Complex amplitude of constant normally incident acoustic pressure[1]
$\hat{p}_r$ = Complex amplitude of normally reflected acoustic pressure, = $\hat{p}_i-(\rho_0 c/S)\hat{U}_{\mathrm{I}}$
$\hat{p}_t$ = Complex amplitude of normally transmitted acoustic pressure, = $(\rho_0 c/S)\hat{U}_{\mathrm{II}}$
R = Complex pressure-amplitude reflection coefficient, = $1-(\rho_0 c/S)(\hat{U}_{\mathrm{I}}/\hat{p}_i)$
R_E = Electrical resistance of voice coil in moving-coil actuator
R_g = Output resistance of electrical control source (signal generator)
R_{Mn} = Effective mechanical resistance of nth module element
R_{Mmn} = Effective mechanical resistance coupling mth and nth module elements ($m \neq n$)
S = Total cross-sectional area of ASP modules and hypothetical source and receiving space plane-wave tubes, = $S_1+S_2 = S_3+S_4$

S_n = Cross-sectional area of nth module element
TL = Normal-incidence sound transmission loss, $= 10\log(1/\tau)$
$\hat{u}_n$ = Complex normal velocity amplitude of nth module element
$\hat{U}_{\mathrm{I}}$ = Volume velocity on side I (source side) of module
$\hat{U}_{\mathrm{II}}$ = Volume velocity on side II (transmitting side) of module
Z_{A1} = Acoustic impedance substitution for waveguide two-port network, $= j(\rho_0\omega/\tilde{k}S)\tan(\tilde{k}L/2) \approx j(\rho_0 c/S)\tan(kL/2)$
Z_{A2} = Acoustic impedance substitution for two-port waveguide network, $= -j(\rho_0\omega/\tilde{k}S)\csc(\tilde{k}L) \approx -j(\rho_0 c/S)\csc(kL)$
Z_{A3} = Acoustic impedance substitution, $= Z_{A1}+Z_{A2}+(\rho_0 c/S)$
Z_{A4} = Acoustic impedance substitution, $= Z_{A3} - [Z_{A2}^2(Z_{M3}S_4^2+Z_{M4}S_3^2+Z_{M34}S^2)]/[(Z_{M3}S_4^2+Z_{M4}S_3^2+Z_{M34}S^2)Z_{A3}+Z_{M3}Z_{M4}+(Z_{M3}+Z_{M4})Z_{M34}]$
Z_E = Isolated electric impedance of moving-coil actuator and electrical control source output,$= R_g+R_E+j\omega L_E$
Z_{Mn} = Effective mechanical impedance of nth module element, $=\begin{cases} j\omega M_{Mn};\ n=1,\text{for module configurations 1 and 4} \\ R_{Mn}+j[\omega M_{Mn}-(1/\omega C_{Mn})];\ \text{otherwise} \end{cases}$
Z_{Mmn} = Effective mechanical impedance coupling mth and nth module elements $(m \neq n)$, $= R_{Mmn}+(1/j\omega C_{M\mathrm{mn}})$
α = Total thermoviscous absorption coefficient for acoustic losses in module cavities[2]
δ = In-plane width of thin transmitting surface
ρ_0 = Ambient density of fluid medium
σ_{Mn} = Effective mass surface density of nth element, $= M_{Mn}/S_n$
τ = Sound power transmission coefficient
ω = Angular frequency, $= 2\pi f$

I. INTRODUCTION

An active segmented partition (ASP) is a contiguous array of interconnected modules or elements that are actively controlled to reduce sound transmission between a source space and a receiving space. While limited investigations of ASPs have been conducted over the past few years,[3–16] in-depth comparative analyses of individual ASP module configurations are still needed to better understand their behaviors and to establish those that produce the highest transmission loss using simple control strategies.

A discrete ASP module is a complete subsection of an array, consisting of an integrated arrangement of active and passive components that are often acoustically and structurally small. If a module is well designed and controlled, it interacts with adjacent modules and supporting structures to yield effective control of sound transmission through the entire partition. Moreover, because an ASP typically consists of several identical modules, individual module design governs overall partition performance, as does the method of control, the method of structural support, and the method of module interconnection. Inadequate attention to any of these details can lead to serious performance limitations (at least over substantial bandwidths) or relegate the approach to use with impractical control schemes.

Much of the past research in active sound transmission control (ASTC) has focused on difficulties of simultaneously controlling distributed structural and fluid media, and has essentially dismissed active vibration control of partitions as an effective means of controlling sound transmission.[17–22] The research has instead emphasized restructuring of distributed partition modes (rather than suppression of modes) to produce normal surface velocity distributions that transmit inefficiently into receiving spaces.[23] Nevertheless, researchers have found that effective reduction of sound transmission is generally accomplished by both partition modal amplitude reduction and modal restructuring,[24] with the weight of each mechanism depending upon specific geometric and structural-acoustic parameters.[5,25–27] As a result, the notion that active suppression of partition vibration yields ineffective control of sound transmission should not necessarily be applied as a generalization to all types of partitions.

Many complexities of distributed partition ASTC that have discounted vibration control methods result from a common condition in which secondary control force or moment distributions fail to match corresponding distributions produced by primary incident pressure disturbances. However, local physical conditions differ significantly for partitions segmented into small, discretely controlled components. In the case of ASPs, primary and secondary force distributions may be constrained to match more closely on key module surfaces, permitting more efficient simultaneous control of partition vibration and sound transmission. Moreover, efficient global control of transmitting surface vibrations produces sound transmission control applicable to many types of source and receiving spaces—to both their near fields and far fields.

Past ASTC research has also emphasized the behavior and positional optimization of error sensors and actuators in conjunction with active partitions and their surroundings. However, transducer positional optimization schemes are often based on unreliable assumptions of system time invariance. While adaptive controllers are able to modify and optimize control filters for time-varying systems, *a priori* optimized transducer locations must necessarily remain fixed and nonadaptive. What is needed, therefore, is a physical ASTC strategy that performs well for a variety of source and receiving spaces and remains essentially unaffected by their time-varying physical changes.

In recent years, the authors have identified several research considerations to address such needs and to otherwise improve the practicality and performance of ASTC systems. Other efforts have provided tools to conceptualize, model, and evaluate ASP modules, and have led to the proposal of seven criteria for their design and performance.[7,11–13,16] While some research efforts have shown that ASPs may be used to control transmitted volume velocity, sound power, total potential energy, or other receiving space field quantities (typically through elaborate multichannel sensing and

control), the seven criteria suggest that a much simpler scheme based on localized module vibration control may be advantageous.

This paper provides a comparative theoretical and numerical investigation of four ASP modules that were identified as candidates to satisfy the criteria. It explores their salient properties and a practical vibration-based scheme to control them. It compares normal-incidence transmission loss and reflection coefficient estimates for the modules in their passive and active states. The transmission loss estimates are well suited for comparison with classical normal-incidence transmission loss formulations. The analysis reveals basic problems and performance limitations for some configurations, and provides recommendations that may be used to enhance their effectiveness. It also identifies mechanisms of higher-performance vibration-controlled ASPs to enhance the viability of ASPs as ASTC solutions.

The underlying active control objective for each module is to induce global vibration control of its various transmitting surfaces by directly minimizing normal vibration of its *principal* transmitting surface. The analysis shows why single-composite-leaf (SCL) ASP modules are typically unable to use this simple strategy effectively. It then introduces two double-composite-leaf (DCL) modules that use the strategy much more effectively to produce efficient global vibration control of transmitting surfaces and achieve high transmission loss over a broad frequency range. One module is especially noteworthy in that it is designed to enhance implementation of full ASP arrays while satisfying the seven design and performance criteria mentioned above.

The investigation explores physical configurations of individual ASP modules rather than complete ASP arrays. However, it does so while acknowledging basic array requirements and characteristics. Results are derived assuming the use of moving-coil actuators, but they are representative of results based on other transducer formats. One-dimensional acoustic fields, lumped mechanical elements, analogous electro-mechano-acoustic circuits,[28,29] and time-harmonic excitation and control are employed to efficiently model and evaluate the configurations. Relevant assumptions and simplifications are made to limit otherwise unwieldy circuit diagrams to planar (though still somewhat complicated) forms. These steps are carried out carefully to avoid detracting from key module characteristics.

The following sections present theoretical developments for the four module configurations and numerical examples to illustrate their characteristic behaviors. They also discuss additional ASP module limitations and capabilities from a general standpoint.

II. SELECTED ASP MODULE CONFIGURATIONS

A. Configuration 1: Single composite leaf (SCL) with a surrounding finite-impedance interstice

The first module configuration is shown in Fig. 1. It includes an actuator with its diaphragm and a surrounding interstice to which the actuator frame is connected. Little consideration has previously been given to the effects that actuator control has on supporting ASP structures such as this interstice. A common tacit assumption is that supporting structures have infinite impedance. However, this notion is invalid for actuators supported by many partition elements. When exposed finite-impedance elements form transmitting interstitial components, their vibrations can pose significant ASTC problems.

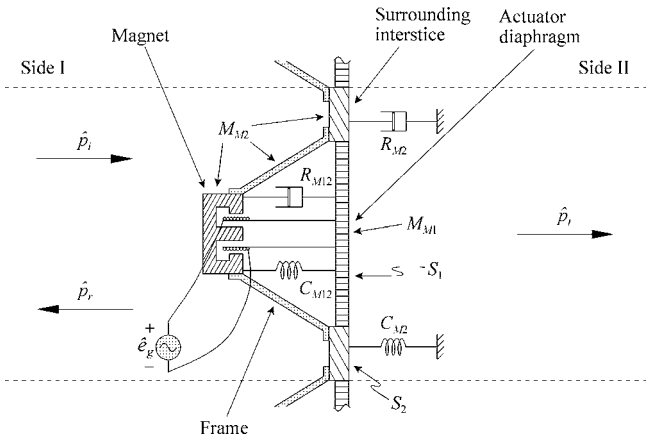

FIG. 1. Isolated view of ASP module configuration 1. An actuator diaphragm vibrates freely but snugly within the frictionless interstice opening. Both the actuator diaphragm and the interstice are assumed to vibrate as pistons in normal translational rigid-body modes. Plane waves are normally incident and reflected in the source space, and normally transmitted in the receiving space. The model isolates effects of acoustic forces and reactive motor forces on the interstice. (After Ref. 7.)

The supporting interstice is assumed to form a single lumped-element system around the periphery of the actuator diaphragm with effective mechanical mass, compliance, and resistance. The diaphragm is assumed to vibrate freely but snugly within its frictionless opening such that no sound can transmit through an intervening crack. Although lumped mechanical resistance and compliance elements are shown on opposite sides of the diaphragm and interstice, they are assumed to apply uniformly over the pertinent cross sections. The interstice and diaphragm are assumed to vibrate only in normal translational rigid-body modes, so the entire transmitting surface area of the module is composed of piston-like elements. The actuator magnet and frame are considered to be acoustically unobtrusive lumped masses that firmly attach to the interstice and vibrate in unison with it.

As suggested by the dashed horizontal lines in the drawing, the semi-infinite source space (side I) and receiving space (side II) are assumed to behave as one-dimensional low-frequency fields, such as those constrained by rigid-walled plane-wave tubes. A constant incident pressure wave impinges normally upon the module from the source space while another wave reflects normally back into the source space. A transmitted wave propagates normally into the receiving space, which has the same characteristic impedance as the source space.

1. Equivalent circuit modeling and analytical results

An equivalent circuit representing the complete system under time-harmonic excitation and control is shown in Fig. 2 (see the List of Symbols for clarification of labels). The circuit includes four ideal area gyrators that couple the me-

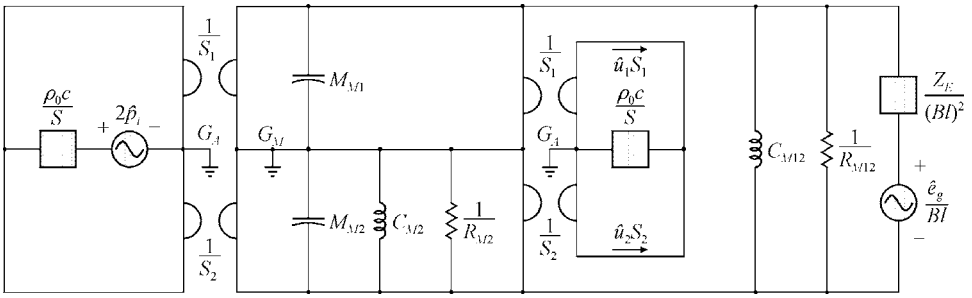

FIG. 2. Multiple-domain equivalent circuit representing ASP module configuration 1. (After Ref. 7.)

chanical mobility portion of the circuit to the acoustic impedance portions, the latter representing the source and receiving spaces. The control voltage input and combined electric impedance of the signal generator and actuator have been carried through an ideal transformer from the electric impedance domain to the mechanical mobility portion of the circuit.

Normal velocity amplitudes of the actuator diaphragm ($\hat{u}_1$) and the surrounding interstice ($\hat{u}_2$) may be derived directly from the circuit by (1) writing the defining equations for the ideal gyrators and ensuring they are satisfied with appropriate flow and potential senses; (2) writing the equations of motion in all physical domains using Kirchhoff's flow law (i.e., writing the nodal equations for all nodes except the ground reference nodes); and (3) solving the simultaneous algebraic equations for the velocities. Four nodal equations for the model reduce to two coupled equations of motion for the diaphragm and interstice, yielding the two complex amplitudes. They are functions of both incident pressure and electrical input voltage

$$\hat{u}_1 = \frac{2\hat{p}_i\left\{Z_{M2}S_1 + \left[Z_{M12} + \frac{(Bl)^2}{Z_E}\right]S\right\} + \hat{e}_g\frac{Bl}{Z_E}(2\rho_0 c S_2 + Z_{M2})}{\left[2\frac{\rho_0 c}{S}S_1^2 + Z_{M1} + Z_{M12} + \frac{(Bl)^2}{Z_E}\right]\left[2\frac{\rho_0 c}{S}S_2^2 + Z_{M2} + Z_{M12} + \frac{(Bl)^2}{Z_E}\right] - \left[2\frac{\rho_0 c}{S}S_1 S_2 - Z_{M12} - \frac{(Bl)^2}{Z_E}\right]^2}, \tag{1}$$

$$\hat{u}_2 = \frac{2\hat{p}_i\left\{Z_{M1}S_2 + \left[Z_{M12} + \frac{(Bl)^2}{Z_E}\right]S\right\} - \hat{e}_g\frac{Bl}{Z_E}(2\rho_0 c S_1 + Z_{M1})}{\left[2\frac{\rho_0 c}{S}S_1^2 + Z_{M1} + Z_{M12} + \frac{(Bl)^2}{Z_E}\right]\left[2\frac{\rho_0 c}{S}S_2^2 + Z_{M2} + Z_{M12} + \frac{(Bl)^2}{Z_E}\right] - \left[2\frac{\rho_0 c}{S}S_1 S_2 - Z_{M12} - \frac{(Bl)^2}{Z_E}\right]^2}. \tag{2}$$

The total volume velocity produced by the vibrating surfaces is the same on both sides of the module:

$$\hat{U}_{\mathrm{I}} = \hat{U}_{\mathrm{II}} = \hat{u}_1 S_1 + \hat{u}_2 S_2 = \frac{2\hat{p}_i\left\{Z_{M1}S_2^2 + Z_{M2}S_1^2 + \left[Z_{M12} + \frac{(Bl)^2}{Z_E}\right]S^2\right\} + \hat{e}_g\frac{Bl}{Z_E}(Z_{M2}S_1 - Z_{M1}S_2)}{\left[2\frac{\rho_0 c}{S}S_1^2 + Z_{M1} + Z_{M12} + \frac{(Bl)^2}{Z_E}\right]\left[2\frac{\rho_0 c}{S}S_2^2 + Z_{M2} + Z_{M12} + \frac{(Bl)^2}{Z_E}\right] - \left[2\frac{\rho_0 c}{S}S_1 S_2 - Z_{M12} - \frac{(Bl)^2}{Z_E}\right]^2}. \tag{3}$$

This result is used to determine the transmitted pressure, sound power transmission coefficient, transmission loss, and source-side pressure-amplitude reflection coefficient under both passive and active conditions.

Under open-circuit passive conditions, $Z_E \to \infty$ and the inverse transmission coefficient becomes[30]

$$\frac{1}{\tau} = \left|\frac{\left(2\frac{\rho_0 c}{S}S_1^2 + Z_{M1} + Z_{M12}\right)\left(2\frac{\rho_0 c}{S}S_2^2 + Z_{M2} + Z_{M12}\right) - \left(2\frac{\rho_0 c}{S}S_1 S_2 - Z_{M12}\right)^2}{2\frac{\rho_0 c}{S}(Z_{M1}S_2^2 + Z_{M2}S_1^2 + Z_{M12}S^2)}\right|^2. \tag{4}$$

The reflection coefficient becomes

$$R = 1 - 2\frac{\rho_0 c}{S}\left[\frac{Z_{M1}S_2^2 + Z_{M2}S_1^2 + Z_{M12}S^2}{\left(2\frac{\rho_0 c}{S}S_1^2 + Z_{M1} + Z_{M12}\right)\left(2\frac{\rho_0 c}{S}S_2^2 + Z_{M2} + Z_{M12}\right) - \left(2\frac{\rho_0 c}{S}S_1 S_2 - Z_{M12}\right)^2}\right]. \tag{5}$$

As stated in Sec. I, the active control strategy for the configuration is to minimize the normal velocity of its principal transmitting surface: the actuator diaphragm. Equation (1) demonstrates that it may be driven to zero (assuming sufficient actuator power handling and linear response) using the following input control voltage:

$$\hat{e}_g = -2\hat{p}_i\frac{Z_E}{Bl}\left\{\frac{Z_{M2}S_1 + \left[Z_{M12} + \frac{(Bl)^2}{Z_E}\right]S}{2\rho_0 c S_2 + Z_{M2}}\right\}. \tag{6}$$

However, forces due to the impinging incident wave, coupling, and reaction of the actuator motor against the finite impedance interstice will cause it to vibrate with velocity amplitude

$$\hat{u}_2 = \frac{2\hat{p}_i(S_1 + S_2)}{2\rho_0 c S_2 + Z_{M2}}. \tag{7}$$

The force due to incident pressure on the actuator diaphragm is accordingly transferred by the actuator motor to the surrounding interstice. The residual volume velocity $\hat{U}_{\mathrm{II}} = \hat{u}_2 S_2$ leads to the controlled inverse transmission coefficient

$$\frac{1}{\tau} = \left|1 + \frac{Z_{M2}}{2\rho_0 c S_2}\right|^2. \tag{8}$$

Significantly, this expression is the same as that resulting from a *passive* single-leaf partition with mechanical impedance Z_{M2} and transmitting surface area S_2, instead of total surface area $S = S_1 + S_2$.

When the interstice is mass controlled, the reciprocal transmission coefficient becomes

$$\frac{1}{\tau} \approx 1 + \left(\frac{\omega\sigma_{M2}}{2\rho_0 c}\right)^2, \tag{9}$$

which corresponds to the normal-incidence mass law for a homogeneous single-leaf partition of surface density σ_{M2}. Notably, the interstice mass M_{M2} includes the mass of the actuator magnet and frame. Hence, this result shows that when the interstice is mass controlled, the active control scheme provides no added benefit to that which could be achieved by a *passive* module constructed solely of the interstitial material with a mass equivalent to that of the actuator magnet and frame added to it.

Equation (8) reveals several other noteworthy properties. First, it indicates that the transmission loss of the controlled module depends upon the interstice surface area and not the diaphragm surface area. Second, it shows that the transmission loss is independent of the actuator diaphragm mass. Hence, the configuration could employ any piston-like diaphragm with appropriate dimensions. Third, it demonstrates that transmission loss increases with increased interstice impedance. For a lightweight ASP, the interstice does not necessarily have to be massive to have high impedance in the direction normal to the partition. It might be oriented so that it is deeper from the source side to the receiving side and proportionately narrower in the plane of the partition. This would significantly increase stiffness in the direction normal to the partition without increasing mass. It would also produce the simultaneous benefit of decreasing the transmitting interstice surface area S_2, which as seen in Eq. (8) would increase transmission loss even more.

Another important property of the controlled configuration is its pressure-amplitude reflection coefficient R as seen from the source space. If $|R| > 1$, the module adds energy to the semi-infinite one-dimensional field, at least relative to that encountered in the presence of a perfectly rigid boundary. On the other hand, if $|R| < 1$, it absorbs at least a portion of the incident energy.[31] Thus, to avoid exacerbating noise levels in the primary field, a desirable requirement might simply be that $|R| \leqslant 1$. The reflection coefficient determined from the residual volume velocity $\hat{U}_{\mathrm{I}}$ is

$$R = \frac{Z_{M2}}{2\rho_0 c S_2 + Z_{M2}}, \tag{10}$$

which satisfies this requirement. In the high-frequency limit (i.e., when the interstice is fully mass controlled), $R \to 1$.

Based on these analyses, it appears that if one could make the interstitial surface area vanishingly small and its normal stiffness extremely large, the sound transmission through the controlled module would become correspondingly small. However, Sec. II B discusses an important detail that has been neglected and that significantly limits the performance of realizable SCL configurations.

2. Numerical example

Table I provides several numerical values for a representative example of the configuration. The parameters are used with Eqs. (4) and (8) to generate normal-incidence transmis-

TABLE I. Parameter values used in the numerical example for ASP module configuration 1.

Parameter	Value	Parameter	Value
Bl	5 T·m	R_g	0.1 Ω
c	343 m/s	R_{M2}	3 kg/s
C_{M2}	200 μm/N	R_{M12}	1 kg/s
C_{M12}	500 μm/N	S	400 cm^2
L_E	0.5 mH	S_1	75 cm^2
M_{M1}	7 g	S_2	325 cm^2
M_{M2}	325 g	ρ_0	1.21 kg/m^3
R_E	6 Ω		

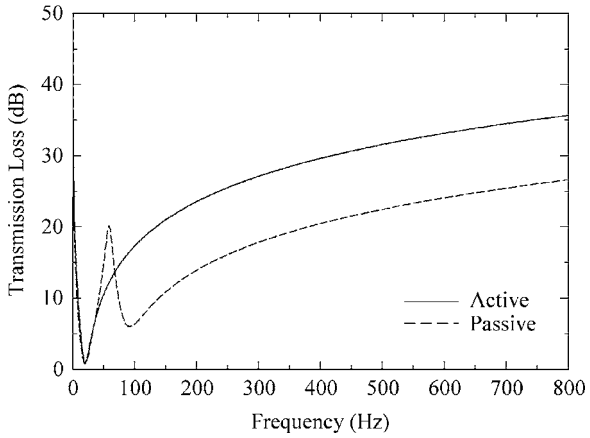

FIG. 3. Normal-incidence transmission loss for ASP module configuration 1 under open-circuit passive and active conditions (calculated using numerical values from Table I).

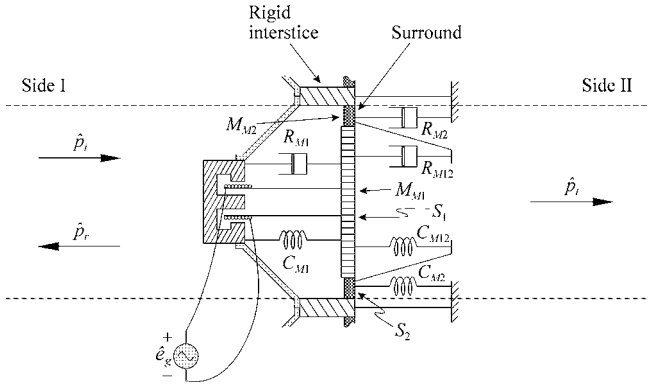

FIG. 5. Isolated view of ASP module configuration 2. An actuator diaphragm is connected to a surrounding resilient suspension, which is connected on its opposite side to a stiffened interstice. The surround is represented with lumped mechanical elements. The model isolates effects of acoustic forces and diaphragm forces on the resilient surround. (After Ref. 7.)

sion loss curves for passive and active conditions, as shown in Fig. 3. As the curves demonstrate, control of sound transmission is poor for both states at lower audible frequencies. However, performance gradually improves to modest levels at higher frequencies. Active control produces a 9-dB improvement over passive control at these higher frequencies, but it performs no better at very low frequencies and actually performs worse in the narrow band centered at 58 Hz.

The values in Table I are also used with Eqs. (5) and (10) to provide a similar comparison of source-side reflection coefficient moduli under passive and active conditions (see Fig. 4). In both Figs. 3 and 4, curve dips correspond to resonances of vibrating module elements. The dip centered at 87 Hz for the passive condition corresponds to the resonance of the resiliently mounted diaphragm. Because the diaphragm motion is minimized via active control, this dip vanishes in the active state. The dip centered at 20 Hz for both passive and active conditions corresponds to the dominant resonance of the interstice (with the mounted actuator).

B. Configuration 2: Single-composite leaf (SCL) with a surrounding suspension

The analysis of the first module configuration assumed the actuator diaphragm vibrated freely but snugly within the surrounding interstice opening so that no sound could transmit through an intervening crack. In practice, this idealized behavior would be extremely difficult to achieve. An airtight seal between an actuator diaphragm and a surrounding interstice would be realized with a mechanical connection. This connection must be resilient to produce sufficient suspension compliance and reduce undesirable mechanical coupling between adjacent ASP elements (a presumed requirement for controller simplification). A compliant airtight suspension with finite transmitting surface area is therefore introduced between the diaphragm and interstice as shown in Fig. 5. This suspension is analogous to the surround of a typical moving-coil loudspeaker. When used in conjunction with an adequately spaced rear suspension (e.g., a spider), it forms a composite dual suspension that significantly restricts diaphragm motion to translational rigid-body motion. As a transmitting surface, a surrounding suspension possesses degrees of vibrational freedom that may be difficult to control. Since it responds somewhat independently to impinging sound waves, a knowledge of its behavior is crucial to understand the performance of the module when the normal velocity of the transmitting diaphragm is minimized through actuation.

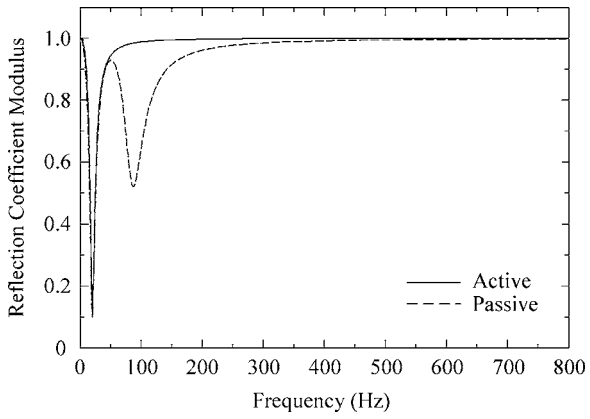

FIG. 4. Source-side reflection coefficient modulus for ASP module configuration 1 under open-circuit passive and active conditions (calculated using numerical values from Table I).

1. Equivalent circuit modeling and analytical results

For this model, the interstice is assumed to have infinite stiffness in the direction normal to the partition plane, and its in-plane area is assumed to be negligible.[33] As a result, dominant effects of the suspension are well isolated and a useful representation of the module is given by the equivalent circuit in Fig. 6. The surrounding suspension is modeled as a lumped mass connected between the actuator diaphragm and the rigid interstice with compliance and resistance on both sides. Solving the circuit as described in Sec. II A 1, produces the following normal surface velocities for the diaphragm and surround:

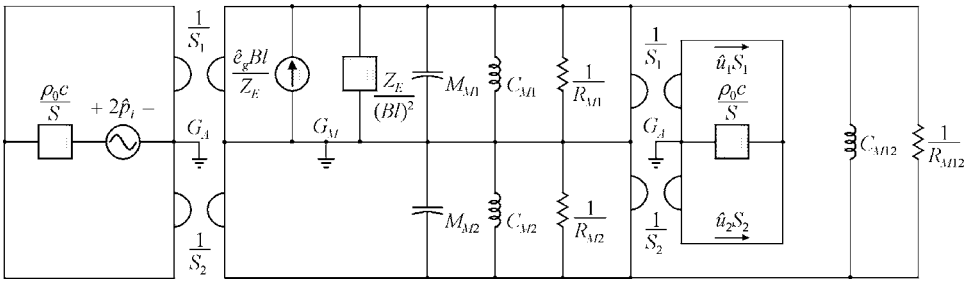

FIG. 6. Multiple-domain equivalent circuit representing ASP module configuration 2. (After Ref. 7.)

$$\hat{u}_1 = \frac{2\hat{p}_i(Z_{M2}S_1 + Z_{M12}S) + \hat{e}_g\frac{Bl}{Z_E}\left(2\frac{\rho_0 c}{S}S_2^2 + Z_{M2} + Z_{M12}\right)}{\left[2\frac{\rho_0 c}{S}S_1^2 + Z_{M1} + \frac{(Bl)^2}{Z_E} + Z_{M12}\right]\left(2\frac{\rho_0 c}{S}S_2^2 + Z_{M2} + Z_{M12}\right) - \left(2\frac{\rho_0 c}{S}S_1S_2 - Z_{M12}\right)^2}, \tag{11}$$

$$\hat{u}_2 = \frac{2\hat{p}_i\left\{\left[Z_{M1} + \frac{(Bl)^2}{Z_E}\right]S_2 + Z_{M12}S\right\} - \hat{e}_g\frac{Bl}{Z_E}\left(2\frac{\rho_0 c}{S}S_1S_2 - Z_{M12}\right)}{\left[2\frac{\rho_0 c}{S}S_1^2 + Z_{M1} + \frac{(Bl)^2}{Z_E} + Z_{M12}\right]\left(2\frac{\rho_0 c}{S}S_2^2 + Z_{M2} + Z_{M12}\right) - \left(2\frac{\rho_0 c}{S}S_1S_2 - Z_{M12}\right)^2}. \tag{12}$$

The total volume velocity is then

$$\hat{U}_{\mathrm{I}} = \hat{U}_{\mathrm{II}} = \frac{2\hat{p}_i\left\{\left[Z_{M1} + \frac{(Bl)^2}{Z_E}\right]S_2^2 + Z_{M2}S_1^2 + Z_{M12}S^2\right\} + \hat{e}_g\frac{Bl}{Z_E}(Z_{M2}S_1 + Z_{M12}S)}{\left[2\frac{\rho_0 c}{S}S_1^2 + Z_{M1} + \frac{(Bl)^2}{Z_E} + Z_{M12}\right]\left(2\frac{\rho_0 c}{S}S_2^2 + Z_{M2} + Z_{M12}\right) - \left(2\frac{\rho_0 c}{S}S_1S_2 - Z_{M12}\right)^2}. \tag{13}$$

While this configuration is notably different than configuration 1, its analytical representations for passive $1/\tau$ and R are identical to those given in Eqs. (4) and (5) (except that the definition of Z_{M1} differs as shown in the List of Symbols). The control voltage required to drive the normal diaphragm velocity $\hat{u}_1$ to zero is

$$\hat{e}_g = -2\hat{p}_i\frac{Z_E}{Bl}\left(\frac{Z_{M2}S_1 + Z_{M12}S}{2\frac{\rho_0 c}{S}S_2^2 + Z_{M2} + Z_{M12}}\right). \tag{14}$$

When it is applied, the normal surround velocity becomes

$$\hat{u}_2 = \frac{2\hat{p}_iS_2}{2\frac{\rho_0 c}{S}S_2^2 + Z_{M2} + Z_{M12}}. \tag{15}$$

The resulting volume velocity for the controlled condition then produces the inverse transmission coefficient

$$\frac{1}{\tau} = \left|1 + \frac{Z_{M2} + Z_{M12}}{2\frac{\rho_0 c}{S}S_2^2}\right|^2. \tag{16}$$

If the surround becomes mass controlled, $Z_{M2}+Z_{M12} \approx j\omega M_{M2}=j\omega\sigma_{M2}S_2$ and the inverse transmission coefficient becomes

$$\frac{1}{\tau} \approx 1 + \left(\frac{\omega\sigma_{M2}}{2\rho_0 c}\right)^2\left(\frac{S}{S_2}\right)^2. \tag{17}$$

The reflection coefficient for the controlled configuration is given by the relationship

$$R = \frac{Z_{M2} + Z_{M12}}{2\frac{\rho_0 c}{S}S_2^2 + Z_{M2} + Z_{M12}}. \tag{18}$$

This once again satisfies the requirement that $|R| \leqslant 1$ and in the high-frequency limit, $R \to 1$.

The results given above indicate that the ways to reduce sound transmission through the resilient surround are (1) to reduce its relative surface area and (2) to increase its mechanical impedance. However, increasing its mechanical mass, stiffness, or resistance has important disadvantages. Dramatically increasing its mass is not a good option if one is trying to minimize overall partition mass. The amount that its stiffness or resistance can be increased will likewise be restricted if the surround is to remain sufficiently resilient. Thus, although these quantities may be increased within prescribed limits, the most important approach to reducing

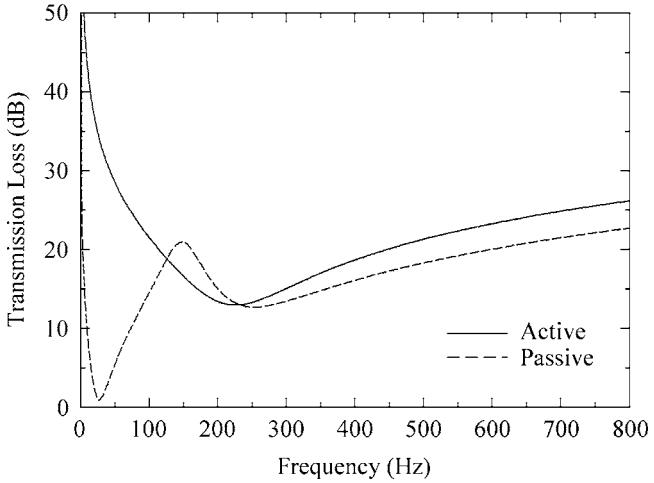

FIG. 7. Normal-incidence transmission loss for ASP module configuration 2 under open-circuit passive and active conditions (calculated using numerical values from Table II).

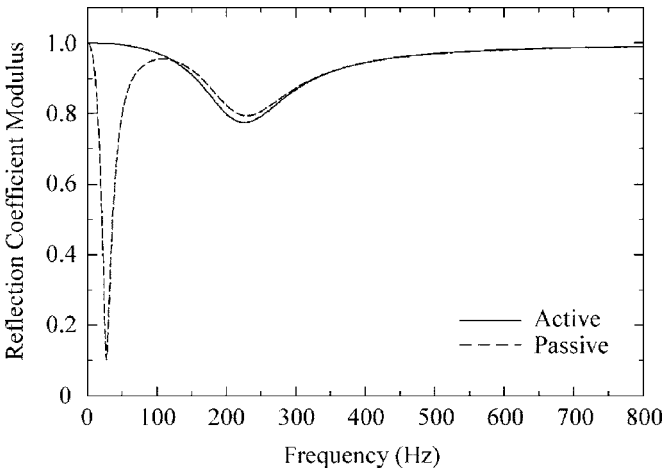

FIG. 8. Source-side reflection coefficient modulus for ASP module configuration 2 under open-circuit passive and active conditions (calculated using numerical values from Table II).

transmission through the surround is to minimize its exposed surface area. This too has practical limitations.

2. Numerical example

Figure 7 uses the analytical results and the parameter values listed in Table II to provide a numerical comparison of the module transmission loss under open-circuit passive and active conditions. Figure 8 provides a similar comparison of the source-side reflection coefficient moduli. In the passive curves of both figures, deep dips centered at 27 Hz are caused by the dominant resonance of the resiliently suspended diaphragm. The shallower and broader dips centered near 235 Hz are produced by the dominant surround resonance. Active control minimizes diaphragm motion, resulting in significant improvement to transmission loss at lower frequencies. However, since the surround remains free to vibrate, the dips near 235 Hz persist. In addition, from 125 to 225 Hz, active control produces transmission loss that is less than that produced by passive control. A comparison of Figs. 3 and 7 also reveals that this active module configuration performs better than configuration 1 at low frequencies (i.e., below 125 Hz) but worse at higher frequencies.

TABLE II. Parameter values used in the numerical example for ASP module configuration 2.

Parameter	Value	Parameter	Value
Bl	5 T·m	R_g	0.1 Ω
c	343 m/s	R_{M1}	2 kg/s
C_{M1}	400 μm/N	R_{M2}	2 kg/s
C_{M2}	200 μm/N	R_{M12}	2 kg/s
C_{M12}	200 μm/N	S	400 cm^2
L_E	0.5 mH	S_1	325 cm^2
M_{M1}	175 g	S_2	75 cm^2
M_{M2}	5 g	ρ_0	1.21 kg/m^3
R_E	6 Ω		

C. Configuration 3: Double-composite leaf (DCL) with acoustic transmitting surface actuation

The preceding sections have provided useful guidelines to increase transmission loss through interstices and actuator diaphragm assemblies. However, they have also shown that the vibration-controlled SCL modules are significantly limited in the ASTC performance they can achieve. Because of this limitation and other problems associated with their incorporation into ASP arrays, the authors chose to explore several other module configurations.[13]

One noteworthy configuration is depicted in Fig. 9. It is a DCL arrangement that incorporates many of the ideas discussed for the preceding configurations but also adds interesting new features. It includes an actuator with a piston-like diaphragm and surround. The actuator frame is rigidly mounted to a stiffened surrounding interstice. Because the interstice impedance normal to the partition is extremely large (assumed to be infinite) and the exposed transmitting surface area is very small, its vibration and contribution to sound transmission are considered negligible. The actuator

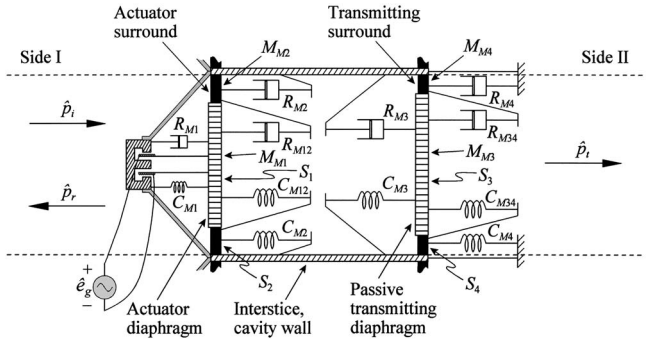

FIG. 9. Isolated view of ASP module configuration 3. An actuator diaphragm is connected to a surrounding resilient suspension, which is connected on its opposite side to a stiffened interstice. The surround is modeled with lumped mechanical elements. A passive transmitting diaphragm is similarly supported by a surrounding resilient suspension and a spaced rear suspension. The source and transmitting sides of the module are separated and acoustically coupled by a small isolated cavity. The model demonstrates useful methods mechano-acoustic actuation and segmentation.

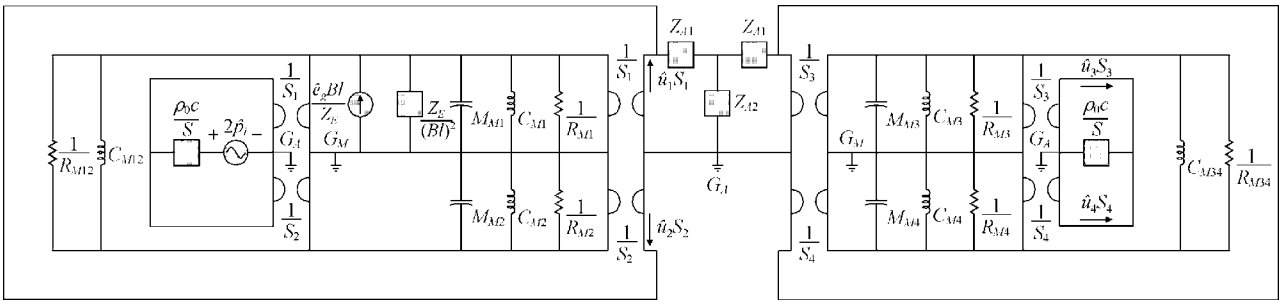

FIG. 10. Multiple-domain equivalent circuit representing ASP module configuration 3.

drives a small sealed cavity to *acoustically* actuate a passive piston-like diaphragm and surround. Both transmitting surfaces are significant. A primary focus of the model is to evaluate the effects of transmitting surround vibration when the module is passive and when its transmitting diaphragm vibration is minimized via active control. As suggested in Sec. II B, performance limitations imposed by transmitting surrounds are difficult to control passively and are therefore of considerable interest. The exposed surface area of the surround may be chosen to be small and its impedance may be chosen to be as large as possible within prescribed limits. The transmitting diaphragm is modeled with connection to both the resilient surround and a spaced rear suspension, the combination helping to constrain its rigid-body translational motion.

1. Equivalent circuit modeling and analytical results

A planar equivalent circuit representing the configuration is shown in Fig. 10. Excitation, radiation, and coupling in the acoustic impedance portions of the circuit are again represented for one-dimensional fields. The simplification neglects higher-order modes and certain near-field coupling effects in the cavity (both of which may merit further analysis), but it acceptably represents cross-sectional spatially averaged field quantities.

Nine nodal equations from the circuit reduce to four coupled equations of motion for the actuator diaphragm, actuator surround, transmitting diaphragm, and transmitting surround, yielding normal surface velocities that are again functions of both incident pressure and electrical input voltage. The velocities of the first two elements combine with their surface areas to produce the following source-side volume velocity:

$$\hat{U}_{\mathrm{I}} = \frac{2\hat{p}_i\left\{\left[Z_{M1} + \frac{(Bl)^2}{Z_E}\right]S_2^2 + Z_{M2}S_1^2 + Z_{M12}S^2\right\} + \hat{e}_g\frac{Bl}{Z_E}(Z_{M2}S_1 + Z_{M12}S)}{\left\{\left[Z_{M1} + \frac{(Bl)^2}{Z_E}\right]S_2^2 + Z_{M2}S_1^2 + Z_{M12}S^2\right\}Z_{A4} + \left[Z_{M1} + \frac{(Bl)^2}{Z_E}\right]Z_{M2} + \left\{\left[Z_{M1} + \frac{(Bl)^2}{Z_E}\right] + Z_{M2}\right\}Z_{M12}}. \tag{19}$$

The normal surface velocities of the transmitting diaphragm and surround are

$$\hat{u}_3 = \hat{U}_{\mathrm{I}}\left[\frac{Z_{A2}(Z_{M4}S_3 + Z_{M34}S)}{(Z_{M3}S_4^2 + Z_{M4}S_3^2 + Z_{M34}S^2)Z_{A3} + Z_{M3}Z_{M4} + (Z_{M3} + Z_{M4})Z_{M34}}\right], \tag{20}$$

and

$$\hat{u}_4 = \hat{u}_3\left(\frac{Z_{M3}S_4 + Z_{M34}S}{Z_{M4}S_3 + Z_{M34}S}\right). \tag{21}$$

These velocities also combine with their surface areas to produce the transmitting volume velocity

$$\hat{U}_{\mathrm{II}} = \hat{U}_{\mathrm{I}}\left(\frac{Z_{A3} - Z_{A4}}{Z_{A2}}\right). \tag{22}$$

Under open-circuit passive conditions, the inverse transmission coefficient then becomes

$$\frac{1}{\tau} = \left|\frac{[(Z_{M1}S_2^2 + Z_{M2}S_1^2 + Z_{M12}S^2)Z_{A4} + Z_{M1}Z_{M2} + (Z_{M1} + Z_{M2})Z_{M12}]Z_{A2}}{2\frac{\rho_0 c}{S}(Z_{M1}S_2^2 + Z_{M2}S_1^2 + Z_{M12}S^2)(Z_{A3} - Z_{A4})}\right|^2, \tag{23}$$

and the source-side reflection coefficient becomes

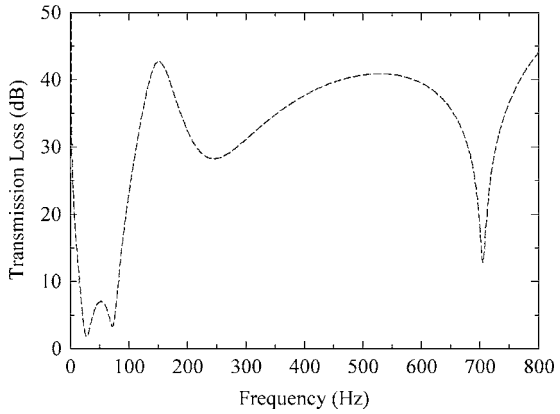

FIG. 11. Normal-incidence transmission loss for ASP module configuration 3 under an open-circuit passive condition (calculated using numerical values from Table III). The predicted infinite transmission loss produced by active control is not plotted.

TABLE III. Parameter values used in the numerical example for ASP module configuration 3.

Parameter	Value	Parameter	Value
Bl	5 T·m	R_E	6 Ω
c	343 m/s	R_g	0.1 Ω
C_{M1}	400 μm/N	R_{M1}	2 kg/s
C_{M2}	200 μm/N	R_{M2}	2 kg/s
C_{M3}	400 μm/N	R_{M3}	2 kg/s
C_{M4}	200 μm/N	R_{M4}	2 kg/s
C_{M12}	200 μm/N	R_{M12}	2 kg/s
C_{M34}	200 μm/N	R_{M34}	2 kg/s
L	25 cm	S	400 cm^2
L_E	0.5 mH	S_1	325 cm^2
M_{M1}	175 g	S_2	75 cm^2
M_{M2}	5 g	S_3	325 cm^2
M_{M3}	175 g	S_4	75 cm^2
M_{M4}	5 g	ρ_0	1.21 kg/m^3

$$R = 1 - 2\frac{\rho_0 c}{S}\left[\frac{Z_{M1}S_2^2 + Z_{M2}S_1^2 + Z_{M12}S^2}{(Z_{M1}S_2^2 + Z_{M2}S_1^2 + Z_{M12}S^2)Z_{A4} + Z_{M1}Z_{M2} + (Z_{M1} + Z_{M2})Z_{M12}}\right]. \tag{24}$$

As seen from Eq. (20), the control strategy of minimizing normal vibration of the transmitting diaphragm is accomplished by driving the *source-side* volume velocity to zero such that $\hat{u}_1 S_1 = -\hat{u}_2 S_2$. Solving Eq. (19) for the required control voltage yields

$$\hat{e}_g = -2\hat{p}_i \frac{Z_E}{Bl}\left\{\frac{\left[Z_{M1} + \frac{(Bl)^2}{Z_E}\right]S_2^2 + Z_{M2}S_1^2 + Z_{M12}S^2}{Z_{M2}S_1 + Z_{M12}S}\right\}. \tag{25}$$

Inspection of Eqs. (21) and (22) further reveals that this voltage and the resulting zero source-side volume velocity simultaneously drive the transmitting surround velocity and the transmitting volume velocity to zero. Thus, with the interstice free from vibration (or otherwise producing negligible sound transmission), the transmission loss of the controlled configuration tends (within modeling constraints) to infinity (i.e., $1/\tau \to \infty$). The source-side reflection coefficient becomes $R = 1$.

2. Numerical example

Figure 11 provides an example of the open-circuit passive transmission loss of the module using the parameters listed in Table III. (The predicted infinite transmission loss is not shown for the active state.) A comparison of passive and active source-side reflection coefficient moduli is given in Fig. 12. The curves show multiple dips corresponding to resonances of the interacting module elements for the open-circuit passive state. Some of these effects are characteristic of common double-leaf partitions, while others result specifically from segmentation. The narrow dip centered at 705 Hz corresponds to the first cavity resonance. The broader dip, centered at about 235 Hz, corresponds to the source-side surround resonance (compare Figs. 7 and 8). As with most passive double-leaf constructions, transmission loss is relatively high at high frequencies, but poor at very low frequencies. Nevertheless, active control produces a substantial increase in transmission loss at all frequencies as long as the module dimensions are small compared with the acoustic wavelength.

D. Configuration 4: Double-composite leaf (DCL) with resilient actuator support

An enhanced DCL configuration is shown in Fig. 13. While it is similar to configuration 3 in many respects, it incorporates a few distinguishing features that improve its integration and control in extended ASP arrays. The actuator frame in configuration 3 was rigidly mounted to the interstice, which was assumed to have infinite impedance. In practice, the interstice impedance would be large but finite.

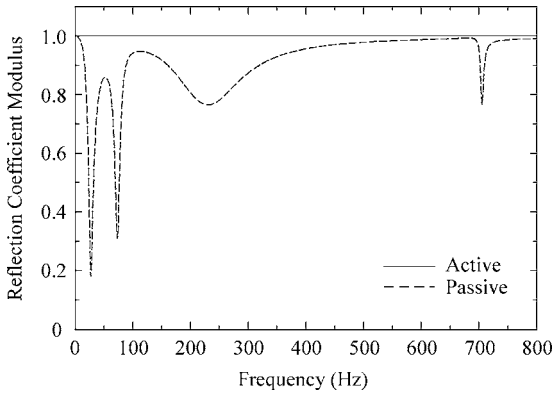

FIG. 12. Source-side reflection coefficient modulus for ASP module configuration 3 under open-circuit passive and active conditions (calculated using numerical values from Table III).

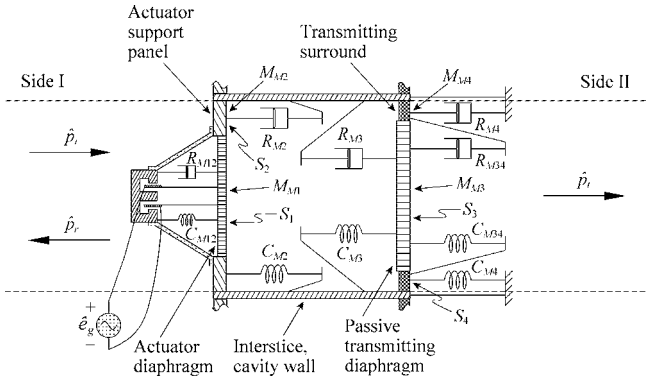

FIG. 13. Isolated view of ASP module configuration 4. An actuator diaphragm vibrates freely but snugly within a frictionless support panel opening. The support panel vibrates similarly within a surrounding interstice opening and is connected to the stiffened interstice by a resilient suspension. A passive transmitting diaphragm is supported by a surrounding resilient suspension and a spaced rear suspension, both modeled with lumped mechanical elements and connected on their opposite sides to the interstice. The source and transmitting sides of the module are separated and acoustically coupled by a small isolated cavity. The model demonstrates useful methods of mechano-acoustic actuation, segmentation, and isolation. (After Ref. 7.)

The reaction of the actuator frame against the interstice would then force it to vibrate to some degree. Configuration 4 accordingly adds a measure of isolation between the actuator and interstice through an inertial support panel. The actuator frame is rigidly mounted to the panel, but the panel is attached to the interstice via a resilient connection. The panel is characterized as a lumped-element piston that vibrates snugly within the frictionless interstice opening. The actuator diaphragm is likewise assumed to vibrate freely but snugly as a piston within the frictionless panel opening, with mechanical resistance and compliance coupling it to the actuator frame.

Sound transmission into the cavity through intervening cracks or surrounds is basically inconsequential. In practice, resilient surrounds must be incorporated with the actuator diaphragm and support panel. However, their areas are neglected here (as with configuration 1) to allow modeling with a planar equivalent circuit. This simplification is acceptable for the source-side elements because, as seen from the analysis of configuration 3, the control condition that minimizes transmitting surface vibrations is a zero source-side volume velocity. Vibration control of the principal transmitting surface and small-cavity acoustic coupling of the transmitting surfaces to the source-side surfaces ensure that the condition is essentially satisfied for any number of source-side surfaces. Hence, the actuator diaphragm and support panel are considered to be the only significant source-side surfaces without much loss in generality.

As with configuration 3, the single actuator controls vibrations of both the transmitting diaphragm and its surround through acoustic actuation. Although the concept of acoustic actuation of *distributed* double-leaf partition cavities is not new,[34–38] important distinctions of this configuration make its actuation and behavior unique in several ways. First, when incorporated into an array, several of these modules form an extended partition that is structurally segmented into isolated elements on both its source side and transmitting side. Both the actuator support panel suspension and the transmitting diaphragm suspension help reduce mechanical coupling to the interstice and adjacent modules. Second, the distinctive pair of diaphragms (actuator diaphragm and transmitting diaphragm) and the actuator support panel vibrate as discrete translation pistons. Third, the actuator diaphragm and support panel produce a zero volume velocity condition on the source side of the cavity. Fourth, the actuator and other elements are configured to produce local cross-sectional symmetries. Fifth, the overall partition cavity is segmented by the interstices into acoustically small cavities. This last characteristic has the important effect of *constraining* primary (noise) and secondary (control) pressure distributions within each cavity, and therefore upon the inner faces of the transmitting diaphragms and surrounds. The pressure distributions are thus compelled to match more closely, yielding improved active control performance.

In reality, acoustic pressure within a cavity is never completely uniform and becomes less uniform with increasing frequency. However, if the transmitting diaphragm is constrained to vibrate only as a translational rigid body, it will respond to the total *spatially averaged* pressure over its cavity-side face. Control of its normal velocity will produce an advantageous effect: the same actuation that minimizes its vibration via spatially averaged pressure will also suppress vibration of the transmitting surround over a broad frequency range. Accordingly, the approach of the configuration is not merely one of acoustic cavity actuation, but an important combination of mechano-acoustic isolation, actuation, and segmentation.

1. Equivalent circuit modeling and analytical results

An equivalent circuit representing the configuration is shown in Fig. 14. Its nine nodal equations again reduce to four coupled equations of motion for the actuator diaphragm, actuator support panel, transmitting diaphragm, and transmitting surround. The velocities and surface areas of the first two elements yield the source-side volume velocity

$$\hat{U}_{\mathrm{I}} = \frac{2\hat{p}_i\left\{ Z_{M1}S_2^2 + Z_{M2}S_1^2 + \left[Z_{M12} + \frac{(Bl)^2}{Z_E} \right] S^2 \right\} + \hat{e}_g \frac{Bl}{Z_E}(Z_{M2}S_1 - Z_{M1}S_2)}{\left\{ Z_{M1}S_2^2 + Z_{M2}S_1^2 + \left[Z_{M12} + \frac{(Bl)^2}{Z_E} \right] S^2 \right\} Z_{A4} + Z_{M1}Z_{M2} + (Z_{M1} + Z_{M2}) \left[Z_{M12} + \frac{(Bl)^2}{Z_E} \right]}. \tag{26}$$

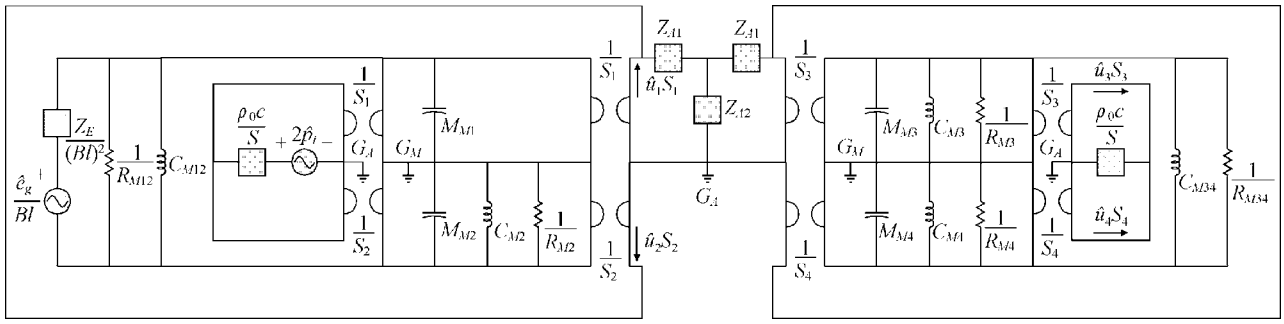

FIG. 14. Multiple-domain equivalent circuit representing ASP module configuration 4. (After Ref. 7.)

Using this result, $\hat{u}_3$, $\hat{u}_4$, and $\hat{U}_{\mathrm{II}}$ are represented as shown in Eqs. (20)–(22). Although the source-side elements are quite different than those of configuration 3, the open-circuit passive representations for $1/\tau$ and R are also identical to those given in Eqs. (23) and (24) (except for the difference in Z_{M1}, as defined in the List of Symbols).

The normal transmitting diaphragm velocity may be driven to zero with the following actuator control voltage:[39]

$$\hat{e}_g = -2\hat{p}_i \frac{Z_E}{Bl}\left\{\frac{Z_{M1}S_2^2 + Z_{M2}S_1^2 + \left[Z_{M12} + \dfrac{(Bl)^2}{Z_E}\right]S^2}{Z_{M2}S_1 - Z_{M1}S_2}\right\}. \tag{27}$$

As indicated earlier, this voltage simultaneously drives the transmitting surround velocity and transmitting volume velocity to zero through the source-side condition $\hat{u}_1 S_1 = -\hat{u}_2 S_2$.[40] The transmission loss thus tends (within modeling constraints) to infinity and the source-side reflection coefficient takes on the constant value of $R=1$. While this reflection coefficient does not reduce acoustic energy in the semi-infinite source space, it does not add energy to the space above that which would occur with a completely rigid boundary.

2. Numerical example

Figure 15 provides an example of the open-circuit passive transmission loss of the module using the parameters listed in Table IV. A comparison of passive and active source-side reflection coefficient moduli is given in Fig. 16. Because of the similarity in module constructions, the curves are similar in some respects to those given in Figs. 11 and 12. Differences follow from the changes to the source-side module elements. Once again, active control produces a considerable increase in transmission loss at all frequencies in which the module dimensions are small compared with the acoustic wavelength.

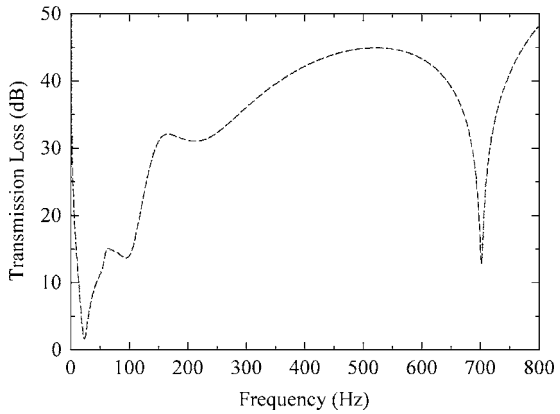

FIG. 15. Normal-incidence transmission loss for ASP module configuration 4 under an open-circuit passive condition (calculated using numerical values from Table IV). The predicted infinite transmission loss produced by active control is not plotted.

3. Design and performance criteria

This module configuration satisfies the seven design and performance criteria mentioned in Sec. I. First, it is designed to utilize simple localized sensors and actuators. This characteristic is important because consistent local control mechanisms allow the module to perform similarly despite changes in adjacent source and receiving spaces. It also allows the module to be self-contained with the possibility of decentralized control. Second, its design and control enable efficient global reduction of normal transmitting surface vibrations (although interstice vibration and transmission are controlled passively). While multiple actuation mechanisms are usually required to control multiple transmitting surface vibrations, this configuration permits efficient control of two vibrating surfaces using only a single actuator. Furthermore, because the control is induced by minimizing vibration of a single transmitting surface, the configuration simplifies error sensing.

TABLE IV. Parameter values used in the numerical example for ASP module configuration 4.

Parameter	Value	Parameter	Value
Bl	5 T·m	R_E	6 Ω
c	343 m/s	R_g	0.1 Ω
C_{M2}	200 μm/N	R_{M2}	3 kg/s
C_{M3}	400 μm/N	R_{M3}	2 kg/s
C_{M4}	200 μm/N	R_{M4}	2 kg/s
C_{M12}	500 μm/N	R_{M12}	1 kg/s
C_{M34}	200 μm/N	R_{M34}	2 kg/s
L	25 cm	S	400 cm^2
L_E	0.5 mH	S_1	75 cm^2
M_{M1}	7 g	S_2	325 cm^2
M_{M2}	325 g	S_3	325 cm^2
M_{M3}	175 g	S_4	75 cm^2
M_{M4}	5 g	ρ_0	1.21 kg/m^3

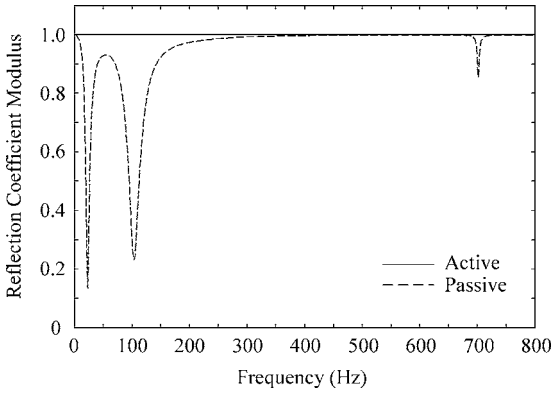

FIG. 16. Source-side reflection coefficient modulus for ASP module configuration 4 under open-circuit passive and active conditions (calculated using numerical values from Table IV).

Third, the configuration may be constructed using appropriate lightweight materials. To ensure lumped-element behavior, key structural elements should be acoustically small and stiffness controlled over frequencies of interest. Fourth, the configuration adds no sound energy to a one-dimensional semi-infinite source space, at least compared to that encountered with a completely rigid boundary. Fifth, the configuration can accommodate simple passive enhancements and function as a hybrid active–passive device. One enhancement of particular interest is the addition of porous absorptive material to the module cavity to improve passive high-frequency transmission loss. The module could then function as an active device at low frequencies, then "cross over" into effective passive control at higher frequencies.

Sixth, the configuration uses small, isolated, lumped-element components with constrained fields and vibrational motions to reduce problems with controllability, observability, and spillover. Seventh, its segmentation and isolation minimize coupling between adjacent partition modules to simplify control requirements and increase the feasibility of decentralized control.

III. ADDITIONAL DISCUSSION OF CAPABILITIES AND LIMITATIONS

The idealized behavior of each module configuration is unavoidably affected by nonideal physical conditions. Some performance limitations result from nonideal vibrational responses. Controlled transmitting components may have residual vibrations or fail to vibrate as ideal rigid bodies. Bending or rotational rigid-body modes ("rocking modes") of transmitting surfaces complicate the behaviors of modules and may reduce their effectiveness. They also affect the assumed accuracy of uniform or spatially averaged pressures employed in equivalent circuits.

Residual vibrations of narrow transmitting surfaces include those of exposed interstices and transmitting diaphragm surrounds. When radiating into a semi-infinite three-dimensional receiving space, these surfaces are similar to baffled annular pistons or strips. Studies of such radiators[41,42] indicate that radiation from a thin interstice or surround becomes very inefficient when its in-plane width δ becomes very small compared to wavelength, i.e., $k\delta \ll 1$. Furthermore, it can be shown[41] that reducing δ while holding the characteristic cross-sectional dimension a of a module constant has greater impact on radiation reduction than reducing a by the same factor with δ held constant. Moreover, with a fixed-dimension array of many modules, minimizing δ remains the only practical method of surface area reduction.

Three of the module configurations in this investigation were assumed to incorporate narrow interstices with infinite impedance in the direction normal to the plane of the partition. If a narrow interstice has finite impedance and does vibrate to a degree, its radiation into a receiving space will be inherently inefficient. However, its vibration will also force limited vibration of the adjacent transmitting diaphragm and surround. Despite this problem, the normal vibration of the principal transmitting surface is still controlled with appropriate actuation.

When translational motion of a transmitting rigid body is effectively reduced, low-amplitude residual rocking may persist. Nevertheless, if a baffled transmitting face of a rigid body rocks symmetrically with respect to its center point (i.e., with odd symmetry), it produces zero net volume velocity. Modules should accordingly be designed to ensure that any residual transmitting surface vibrations fall into this category. When transmitting faces of an ASP are small compared to wavelength, such consistent reduction in volume velocity provides beneficial reduction in sound transmission.[9,10,43] Notably, the method described here is more than just volume velocity control involving large, spatially dependent surface velocities. Instead, the approach produces sound transmission control in two steps. First, it significantly suppresses normal vibration of efficiently transmitting modes. Second, it leaves only low-amplitude residual vibration with a distribution that transmits inefficiently into the receiving space.

The ASP design and performance criteria discussed in Sec. II D 3 require that normal vibrations of *all* transmitting surfaces be minimized to the greatest extent possible. Because module configurations 3 and 4 were found to accomplish the task well, they are expected to simultaneously reduce transmission into both receiving space near fields and far fields. However, near fields produced by narrow residually vibrating surfaces and rocking surfaces possess reactive acoustic energy that cannot be wholly neglected. Such residual vibrations must be carefully considered when listeners or acoustic receivers are positioned close to partitions.

Simultaneous control of the source-side reflection coefficient or the source-space sound field may be desirable while an ASP is engaged in controlling sound transmission. Additional actuation mechanisms may be incorporated into modules to help provide this control or help control residual interstice vibration.[13] While the requirements to accomplish these additional tasks make the problem more complex, the concepts could find application in certain sound transmission problems.

It is anticipated that carefully designed ASP modules will function effectively in complete ASP arrays using simple adaptive controllers. Decentralized controllers may require reduction of coupling between adjacent partition modules to weaken cross-coupling control paths (i.e., trans-

fer functions between actuators and error sensors of neighboring modules).[44] Of the module configurations presented in this investigation, configuration 4 appears to be most capable of producing effective isolation.

IV. CONCLUSIONS

This work has provided a theoretical and numerical investigation of several vibration-controlled modules for use in active segmented partitions (ASPs). These partitions consist of physically segmented arrays of acoustically and structurally small modules that may be regulated using adaptive controllers. The control objective for each module was to induce global control of its various normal transmitting surface vibrations by directly minimizing normal vibration of its *principal* transmitting surface. In some cases, passive means were used to control interstitial surface vibrations. Analyses of the modules were realized using electro-mechano-acoustic circuits. While certain simplifying assumptions were required to make the circuits manageable, they clearly demonstrated important module behaviors. Transmission loss estimates from the analyses are well suited for comparison with classical normal-incidence transmission loss formulations.

The investigation has revealed the inability of two characteristic single-composite-leaf (SCL) configurations to simultaneously control vibration of their transmitting diaphragms, resilient suspensions, and partition interstices under the active control scheme. A numerical example showed that the first configuration produced poor active sound transmission control (ASTC) at low frequencies and moderate ASTC at high frequencies. Another example showed that the second configuration improved low-frequency performance but at the expense of high-frequency performance. In both cases, the introduction of active control was shown to *decrease* transmission loss below passive levels at some frequencies.

Despite these limitations, the investigation provided useful recommendations to enhance ASTC capabilities of these and other vibration-controlled configurations. They suggest that lightweight ASPs should incorporate interstices with very high impedance in the direction normal to the partition. Interstitial widths should also be very narrow in the plane of the partition. Resilient transmitting suspensions that connect stiff diaphragms to interstices should likewise be thin in the plane of the partition and have reasonably large impedances (within prescribed limits to maintain desired resiliency).

Two double-composite-leaf (DCL) configurations were introduced that utilize distinctive combinations of acoustic actuation and mechano-acoustic segmentation. In their passive states, both show transmission loss characteristics typical of double-leaf partitions but add other characteristics unique to their segmented natures. In their active states, they efficiently and globally control transmitting surface vibrations to produce high transmission loss over a broad frequency range. Moreover, because of their localized control mechanisms, their performances remain relatively unaffected by typical time-varying changes to surrounding environments. The second of the two configurations incorporates special segmentation and isolation to reduce coupling between adjacent partition modules and enhance the effectiveness of extended arrays using simple decentralized controllers.

This work has shown that appropriate vibration control of properly configured ASP modules can yield effective local control of sound transmission. When incorporated into full partition arrays, these modules have the potential to enhance the practicality and performance of ASTC systems through their straightforward design, implementation, actuation, error sensing, and application to many sound transmission problems.

ACKNOWLEDGMENTS

The authors gratefully acknowledge financial and other support for portions of this work from the Penn State University Graduate Program in Acoustics. They also acknowledge William Thompson, Jr. for helpful discussions regarding the equivalent circuit modeling.

[1]When appropriate (e.g., for analogous circuit modeling), spatially averaged acoustic pressures and particle velocities may be assumed over relevant cross-sectional areas.
[2]L. E. Kinsler, A. R. Frey, A. B. Coppens, and J. V. Sanders, *Fundamentals of Acoustics*, 4th ed. (Wiley, New York, 2000).
[3]J. E. Cole III and M. C. Junger, "Active noise control for machinery enclosures," NSF Final Report U-1944-379F (1991).
[4]D. R. Thomas, P. A. Nelson, and S. J. Elliott, "An experimental investigation into the active control of sound transmission through stiff light composite panels," Noise Control Eng. J. **41**, 273–279 (1993).
[5]D. R. Thomas, P. A. Nelson, R. J. Pinnington, and S. J. Elliott, "An analytical investigation of the active control of the transmission of sound through plates," J. Sound Vib. **181**, 515–539 (1995).
[6]J. E. Cole, K. F. Martini, and A. W. Stokes, "Active noise control for machinery enclosures," NSF Final Report U-2413-393 (1996).
[7]T. W. Leishman and J. Tichy, "A fundamental investigation of the active control of sound transmission through segmented partition elements," Proceedings of Noise-Con 97, University Park, PA, 1997, Vol. **2**., pp. 137–148.
[8]S. L. Sharp, G. H. Koopmann, and W. Chen, "Transmission loss characteristics of an active trim panel," Proceedings of Noise-Con 97, University Park, PA, 1997, Vol. **2**., pp. 149–160.
[9]M. E. Johnson and S. J. Elliott, "Active control of sound radiation from vibrating surfaces using arrays of discrete actuators," J. Sound Vib. **207**, 743–759 (1997).
[10]R. L. St. Pierre, Jr., G. H. Koopmann, and W. Chen, "Volume velocity control of sound transmission through composite panels," J. Sound Vib. **210**, 441–460 (1998).
[11]T. W. Leishman and J. Tichy, "An experimental evaluation of individual partition segment configurations for the active control of sound transmission," J. Acoust. Soc. Am. **104**, Pt. 2, 1776(A) (1998).
[12]T. W. Leishman and J. Tichy, "An experimental investigation of a novel active segmented partition for sound transmission control," J. Acoust. Soc. Am. **105**, Pt. 2, 1156(A) (1999).
[13]T. W. Leishman, "Active control of sound transmission through partitions composed of discretely controlled modules," Ph.D. thesis, The Pennsylvania State University, University Park, PA, 2000.
[14]S. M. Hirsch, J. Q. Sun, and M. R. Jolly, "An analytical study of interior noise control using segmented panels," J. Sound Vib. **231**, 1007–1021 (2000).
[15]S. M. Hirsch, N. E. Meyer, M. A. Westervelt, P. King, F. J. Li, M. V. Petrova, and J. Q. Sun, "Experimental study of smart segmented trim panels for aircraft interior noise," J. Sound Vib. **231**, 1023–1027 (2000).
[16]T. W. Leishman, "Vibration-controlled modulues for use in active segmented partitions," J. Acoust. Soc. Am. **114**, Pt. 2, 2385(A) (2003).
[17]C. R. Fuller, V. L. Metcalf, R. J. Silcox, and D. E. Brown, "Experiments on structural control of sound transmitted through an elastic plate," Proceedings of the 1989 American Control Conference, Pittsburgh, PA, Vol. **3**, pp. 2079–2084.
[18]C. R. Fuller, "Active control of sound transmission/radiation from elastic

plates by vibration inputs: I. Analysis," J. Sound Vib. **136**, 1–15 (1990).
[19]V. L. Metcalf, C. R. Fuller, R. J. Silcox, and D. E. Brown, "Active control of sound transmission/radiation from elastic plates by vibration inputs. II. Experiments," J. Sound Vib. **153**, 387–402 (1992).
[20]D. R. Thomas, P. A. Nelson, and S. J. Elliott, "Active control of the transmission of sound through a thin cylindrical shell. I. The minimization of vibrational energy," J. Sound Vib. **167**, 91–111 (1993).
[21]D. R. Thomas, P. A. Nelson, and S. J. Elliott, "Active control of the transmission of sound through a thin cylindrical shell. II. The minimization of acoustic potential energy," J. Sound Vib. **167**, 113–128 (1993).
[22]S. D. Snyder and N. Tanaka, "On feedforward active control of sound and vibration using vibration error sensors," J. Acoust. Soc. Am. **94**, 2181–2193 (1993).
[23]C. R. Fuller, C. H. Hansen, and S. D. Snyder, "Active control of sound radiation from a vibrating rectangular panel by sound sources and vibration inputs: An experimental comparison," J. Sound Vib. **145**, 195–215 (1991).
[24]S. D. Snyder and C. H. Hansen, "The design of systems to control actively periodic sound transmission into enclosed spaces. II. Mechanisms and trends," J. Sound Vib. **170**, 451–472 (1994).
[25]S. D. Snyder and C. H. Hansen, "Mechanisms of active noise control by vibration sources," J. Sound Vib. **147**, 519–525 (1991).
[26]J. Pan, C. H. Hansen, and D. A. Bies, "Active control of noise transmission through a panel into a cavity. I. Analytical study," J. Acoust. Soc. Am. **87**, 2098–2108 (1990).
[27]J. Pan and C. H. Hansen, "Active control of noise transmission through a panel into a cavity. II. Experimental study," J. Acoust. Soc. Am. **90**, 1488–1492 (1991).
[28]L. L. Beranek, *Acoustics* (Acoustical Society of America, New York, 1986).
[29]H. F. Olson, *Acoustical Engineering* (Professional Audio Journals, Philadelphia, 1991).
[30]The transmission loss (TL) follows directly from this result as shown in the List of Symbols.
[31]These statements are not necessarily true for enclosed one-dimensional source spaces (Refs. 13 and 32).
[32]T. W. Leishman and J. Tichy, "On the significance of reflection coefficients produced by active surfaces bounding one-dimensional sound fields," J. Acoust. Soc. Am. **113**, 1475–1482 (2003).
[33]Transmission through the interstice is assumed to be completely controlled by its passive characteristics. Active control of interstice vibration is also possible (Ref. 13).
[34]F. W. Grosveld and K. P. Shepherd, "Active sound attenuation across a double wall structure," J. Aircr. **31**, 223–227 (1994).
[35]W. Yamada, T. Sueto, Y. Okudaira, and H. Hamada, "Active control of sound in the cavity of a double wall to increase the sound transmission loss," Proceedings of Inter-Noise 94, Yokohama, Japan, 1994, pp. 1311–1314.
[36]P. Sas, C. Bao, F. Augusztinovicz, and W. Desmet, "Active control of sound transmission through a double panel partition," J. Sound Vib. **180**, 609–625 (1995).
[37]C. Bao and J. Pan, "Experimental study of different approaches for active control of sound transmission through double walls," J. Acoust. Soc. Am. **102**, 1664–1670 (1997).
[38]J. Pan and C. Bao, "Analytical study of different approaches for active control of sound transmission through double walls," J. Acoust. Soc. Am. **103**, 1916–1922 (1998).
[39]This equation corrects Eq. (13) in Ref. 7. Equations (14) and (15) of that paper also have minor errors that may be corrected by solving for $\hat{u}_1$ and $\hat{u}_2$ under general conditions (as outlined in the present paper), then substituting the control voltage.
[40]The concept of minimizing volume velocity into the cavity leads to another possibility for localized error sensing. If the cavity is sufficiently small, it may be feasible to minimize acoustic pressure at a point within the cavity to produce the desired reduction of volume velocity and subsequent control of transmitting surface vibrations. However, the scheme is slightly precarious; it is possible to minimize acoustic pressure at a point in the cavity while the transmitting diaphragm is still vibrating. If small interstice vibrations or extraneous sources in the receiving space cause the transmitting diaphragm to vibrate, the acoustic pressure minimization would not necessarily eliminate sound transmission through the diaphragm and surround. In addition, if a pressure error sensor happened to be located at an uncontrolled pressure node in the cavity, the error signal might not be sufficiently observable and control complications could arise.
[41]W. Thompson, Jr., "The computation of self- and mutual-radiation impedances for annular and elliptical pistons using Bouwkamp's integral," J. Sound Vib. **17**, 221–233 (1971).
[42]S. P. Lipshitz, T. C. Scott, and B. Salvy, "On the acoustic impedance of baffled strip radiators," J. Audio Eng. Soc. **43**, 573–580 (1995).
[43]M. E. Johnson and S. J. Elliott, "Active control of sound radiation using volume velocity cancellation," J. Acoust. Soc. Am. **98**, 2174–2186 (1995).
[44]S. J. Elliott and C. C. Boucher, "Interaction between multiple feedforward active control systems," IEEE Trans. Speech Audio Process. **2**, 521–530 (1994).